PHYSICAL REVIEW B **93**, 201116(R) (2016)

Edge instabilities of topological superconductors

Johannes S. Hofmann,[1,2,*] Fakher F. Assaad,[1] and Andreas P. Schnyder[2,†]

[1]*Institut für Theoretische Physik und Astrophysik, Universität Würzburg, Am Hubland, D-97074 Würzburg, Germany*

[2]*Max-Planck-Institut für Festkörperforschung, Heisenbergstrasse 1, D-70569 Stuttgart, Germany*

(Received 14 December 2015; revised manuscript received 1 April 2016; published 31 May 2016)

Nodal topological superconductors display zero-energy Majorana flat bands at generic edges. The flatness of these edge bands, which is protected by time-reversal and translation symmetry, gives rise to an extensive ground-state degeneracy. Therefore, even arbitrarily weak interactions lead to an instability of the flat-band edge states towards time-reversal and translation-symmetry-broken phases, which lift the ground-state degeneracy. We examine the instabilities of the flat-band edge states of d_{xy}-wave superconductors by performing a mean-field analysis in the Majorana basis of the edge states. The leading instabilities are Majorana mass terms, which correspond to coherent superpositions of particle-particle and particle-hole channels in the fermionic language. We find that attractive interactions induce three different mass terms. One is a coherent superposition of imaginary s-wave pairing and current order, and another combines a charge-density-wave and finite-momentum singlet pairing. Repulsive interactions, on the other hand, lead to ferromagnetism together with spin-triplet pairing at the edge. Our quantum Monte Carlo simulations confirm these findings and demonstrate that these instabilities occur even in the presence of strong quantum fluctuations. We discuss the implications of our results for experiments on cuprate high-temperature superconductors.

DOI: 10.1103/PhysRevB.93.201116

Introduction. The discovery of topological insulators [1,2] has led to the insight that nontrivial band topologies can give rise to exotic surface states [1–3]. Particularly interesting are topological flat-band surface states, since their large density of states enhances correlation effects [4–15]. Surface states with a (nearly) flat dispersion can occur both in topological semimetals [15–17] and in nodal topological superconductors (SCs) [18–21]. However, only in the latter systems is the flatness of the surface states protected by symmetry [21–23]. That is, time-reversal symmetry (TRS), particle-hole symmetry (PHS), and translation symmetry ensure that the surface states are pinned at zero energy, resulting in a band of neutral Majorana fermions.

These Majorana bands exist in one- or two-dimensional regions of the surface Brillouin zone, which are bounded by the projections of the superconducting nodes. Hence, the number of zero-energy surface states grows linearly or quadratically with the length of the system, leading to a diverging density of states at zero energy and an extensive ground-state degeneracy. Since this is in violation with the third law of thermodynamics, even arbitrarily weak interactions cause a singular perturbation of the Majorana flat bands, giving rise to novel symmetry-broken states at the surface [8–15,24]. Due to the flat-band character and the low dimensionality of the boundary, these symmetry-broken states are subject to strong fluctuations. Therefore, it is necessary to use methods beyond mean-field (MF) theory [25] in order to analyze the surface instabilities.

In this Rapid Communication, we employ a mean-field analysis together with continuous-time quantum Monte Carlo (QMC) simulations [26–28] to examine the interaction effects on the Majorana flat-band edge states of d_{xy}-wave superconductors. These edge states are experimentally realized in cuprate high-temperature superconductors [29,30] and have been observed in tunnel junction experiments on normal-metal $YBa_2Cu_3O_{7-x}$ junctions. At intermediate temperatures, these measurements show a sharp zero-bias peak [31–37] that arises due to the diverging density of states of the edge states. Upon further cooling, the observed zero-bias peak splits into two [38,39], which is interpreted as a sign of spontaneous TRS breaking [40]. This was examined by several MF studies [4–9], which found that for attractive interactions the order parameter develops imaginary s-wave components near the boundary, while for repulsive interactions edge ferromagnetism (FM) is induced.

The purpose of this Rapid Communication is to go beyond these previous MF calculations and to conduct a systematic examination of all possible instabilities of the flat-band edge states using (i) a mean-field analysis in the *Majorana basis* of the edge states and (ii) continuous-time QMC simulations which take into account fluctuation effects. Interestingly, we find that for repulsive interactions, the FM instability is coherently mixed with a spin-triplet pairing instability. For attractive interactions, on the other hand, the s-wave pairing instability is combined with current order and similarly the charge-density-wave (CDW) instability, whose wave vector Q corresponds to nesting between the flat bands, is mixed with finite-momentum singlet pairing. We show that for attractive interactions and at half filling, long-range order is established at the edge at $T = 0$. Our findings are relevant for experiments on cuprate high-temperature superconductors and we provide experimental setups to test these unique signatures of Majorana flat bands.

Model. We start from a phenomenological description of a single-band d_{xy}-wave SC given in terms of the Bogoliubov–de Gennes Hamiltonian $\mathcal{H}_0 = \sum_{\mathbf{k}} \Psi_{\mathbf{k}}^\dagger H(\mathbf{k}) \Psi_{\mathbf{k}}$, with the Nambu spinor $\Psi_{\mathbf{k}} = (c_{\mathbf{k}\uparrow}, c_{-\mathbf{k}\downarrow}^\dagger)^{\mathrm{T}}$ and

$$H(\mathbf{k}) = \begin{pmatrix} \varepsilon_{\mathbf{k}} & \Delta_{\mathbf{k}} \\ \Delta_{\mathbf{k}}^* & -\varepsilon_{-\mathbf{k}} \end{pmatrix}. \tag{1}$$

*jhofmann@physik.uni-wuerzburg.de
†a.schnyder@fkf.mpg.de

Here, $c^\dagger_{\mathbf{k}\sigma}$ denotes the electron creation operator with spin σ and momentum $\mathbf{k} = (k_\parallel = k_x, k_\perp = k_y)^{\mathrm{T}}$, anticipating a later introduced ribbon geometry with open boundary conditions in the y direction. The normal part of the Hamiltonian describes a two-dimensional square lattice with nearest-neighbor hopping t and chemical potential μ, hence $\varepsilon_{\mathbf{k}} = -2t\,(\cos k_\parallel + \cos k_\perp) - \mu$. The SC order parameter $\Delta_{\mathbf{k}} = \Delta_{d_{xy}} \sin k_\parallel \sin k_\perp$ contains only spin-singlet pairing of amplitude $\Delta_{d_{xy}}$.

To discuss the topology of this two-dimensional (2D) nodal system, we interpret $H(k_\parallel, k_\perp)$ as a set of fully gapped chains $H_{k_\parallel}(k_\perp)$, indexed by $k_\parallel$. Each subsystem falls into class BDI and its topology is classified by a winding number [19,41–43]. The subsystem exhibits a nontrivial bulk topology if $2|t| > |\mu_{k_\parallel}|$ and $\Delta_{k_\parallel} \neq 0$ and hosts protected zero-energy edge states (created by $\gamma^\dagger_{k_\parallel}$) once open boundary conditions for the perpendicular direction $k_\perp$ are imposed. Here, we use the shorthand notations $\mu_{k_\parallel} = \mu + 2t\cos(k_\parallel)$ and $\Delta_{k_\parallel} = \Delta_{d_{xy}} \sin(k_\parallel)$. The interested reader may find a more detailed discussion of the topology and the protected edge states in Sec. I of Ref. [44].

To study the correlation effects among Majorana states, we include a Hubbard interaction along the top edge ($i_{\perp,0} = 1$) by refining the Hamiltonian to $\mathcal{H} = \mathcal{H}_0 + \mathcal{H}_{\mathrm{int}}$ with

$$\mathcal{H}_{\mathrm{int}} = -\frac{2U}{3L}\sum_{q_\parallel} \mathbf{S}_{-q_\parallel}\mathbf{S}_{q_\parallel} = \frac{2U}{3L}\sum_{q_\parallel} \mathbf{S}^{(\Psi)}_{-q_\parallel}\mathbf{S}^{(\Psi)}_{q_\parallel} \qquad (2)$$

in terms of the physical spin operator $\mathbf{S}_q = \sum_{k_\parallel} c^\dagger_{k_\parallel} \frac{\boldsymbol{\sigma}}{2} c_{k_\parallel+q}$ or a pseudospin operator $\mathbf{S}^{(\Psi)}_q = \sum_{k_\parallel} \Psi^\dagger_{k_\parallel} \frac{\boldsymbol{\tau}}{2} \Psi_{k_\parallel+q}$. Unless stated otherwise, we use $(t, \mu, \Delta_{d_{xy}}, L_\perp) = (1.0, 0.0, 1.0, 10^2)$.

Mean-field considerations. Let us examine some MF decouplings before presenting the numerical simulations. We restrict our discussion to the interacting edge sites and drop the index $i_\perp = i_{\perp,0}$ for readability. All derivations assume half filling $\mu = 0$.

Repulsive interaction. In the presence of repulsive interactions one expects FM instabilities, hence we approximate $\mathcal{H}_{\mathrm{int}}$ by a MF decoupling $\mathbf{m}\mathbf{S}_0$. Projecting on the Majorana states generates the mass term

$$\frac{1}{2}\sum_{k_\parallel=0}^{\pi} \Gamma^\dagger_{k_\parallel} \mathbf{m}_{k_\parallel} \boldsymbol{\tau} \Gamma_{k_\parallel} + \cdots, \qquad (3)$$

with $\Gamma^\dagger_{k_\parallel} = (\gamma^\dagger_{k_\parallel}, -i\, s_{k_\parallel}\, \gamma_{-k_\parallel})$, $s_{k_\parallel} = \mathrm{sgn}(t\,\Delta_{k_\parallel})$, and $\mathbf{m}_{k_\parallel} = \phi^2_{k_\parallel}(i_{\perp,0})\,\mathbf{m}$. The $(\cdots)$ represent edge-bulk and bulk-bulk contributions. This reproduces the edge splitting terms known from Ref. [9]. Due to the $SU(2)$-spin symmetry of the Hamiltonian, the orientation $\mathbf{m}$ remains arbitrary. A nonzero value $|\mathbf{m}|$ breaks time-reversal and spin-rotation symmetry.

To make the connection with the QMC simulations, we express Eq. (3) in terms of fermionic correlations along the edge (see Table I, derived in Sec. II of Ref. [44]). Due to the chiral structure of the edge states, a nonzero mass $|\mathbf{m}|$ corresponds to a coherent superposition of FM and spin-triplet SC, where the in-plane (out-of-plane) components are parallel (antiparallel) aligned. In this analysis, we decomposed the $k_\parallel$ dependence of $\phi^4_{k_\parallel}$ in harmonics. Accordingly, there will be further contributions on next-nearest neighbor and higher-order bonds, oscillating between normal and SC operators.

Attractive interactions. As indicated by Eq. (2), the transformation $c_{\mathbf{k}} \to \Psi_{\mathbf{k}}$ renders $U > 0$ repulsive in terms of $\mathbf{S}^{(\Psi)}_q$. Hence, we expect pseudomagnetic instabilities. First focusing on homogeneous instabilities ($Q = 0$), we find that $\mathbf{S}^{(\Psi)}_0$ projected on the Majorana states is vanishing except for the y component. Therefore, only a condensation of $S^{y,(\Psi)}_0$ gaps the edge spectrum. Including inhomogeneous order (i.e., $Q \neq 0$)

TABLE I. Summary of all possible MF channels at half filling. The top table lists possible vacuum expectation values, their associated masses for the edge states, and the characterizing fermionic correlations. We use $\Gamma^\dagger_{k_\parallel} = (\gamma^\dagger_{k_\parallel}, -i\, s_{k_\parallel}\, \gamma_{-k_\parallel})$ and $\tilde{\Gamma}^\dagger_{k_\parallel} = (\gamma^\dagger_{k_\parallel}, -i\, s_{k_\parallel}\, \gamma^\dagger_{k_\parallel-\pi})$. The $(\cdots)$ indicate additional operators on higher-order bonds.

Nonzero vacuum expectation values	Mass term	Fermionic correlation along interacting edge
$\langle S^{x,y}_0 \rangle$	$\frac{1}{2}\sum_{k_\parallel=0}^{\pi} \Gamma^\dagger_{k_\parallel} m^{x,y}_{k_\parallel} \tau^{x,y} \Gamma_{k_\parallel}$	$\sum_j [a_0 S^{x,y}_j + b_1(\Delta^{b;x,y}_j + \Delta^{b;x,y\,\dagger}_j)] + \cdots$
$\langle S^z_0 \rangle$	$\frac{1}{2}\sum_{k_\parallel=0}^{\pi} \Gamma^\dagger_{k_\parallel} m^z_{k_\parallel} \tau^z \Gamma_{k_\parallel}$	$\sum_j [a_0 S^z_j - b_1(\Delta^{b,z}_j + \Delta^{b,z\,\dagger}_j)] + \cdots$
$\langle S^{x(\Psi)}_\pi \rangle$	$\frac{1}{2}\sum_{k_\parallel=0}^{\pi} \tilde{\Gamma}^\dagger_{k_\parallel} g^x_{k_\parallel} \tau^x \tilde{\Gamma}_{k_\parallel}$	$\sum_j (-1)^j [a_0(\Delta^s_j + \Delta^{s\,\dagger}_j) + b_1 n^b_j] + \cdots$
$\langle S^{y(\Psi)}_0 \rangle$	$\frac{1}{2}\sum_{k_\parallel=0}^{\pi} \tilde{\Gamma}^\dagger_{k_\parallel} (-g^y_{k_\parallel}) \tau^z \tilde{\Gamma}_{k_\parallel}$	$\sum_j [-i a_0(\Delta^s_j - \Delta^{s\,\dagger}_j) + b_1 J_j] + \cdots$
$\langle S^{z(\Psi)}_\pi \rangle$	$\frac{1}{2}\sum_{k_\parallel=0}^{\pi} \tilde{\Gamma}^\dagger_{k_\parallel} g^z_{k_\parallel} \tau^y \tilde{\Gamma}_{k_\parallel}$	$\sum_j (-1)^j [a_0 n_j - b_1(\Delta^{b,s}_j + \Delta^{b,s\,\dagger}_j)] + \cdots$
Operator	**Definitions**	
n_j	$c^\dagger_j \sigma^0 c_j$	
$\mathbf{S}_j$	$c^\dagger_j \frac{\boldsymbol{\sigma}}{2} c_j$	
Δ^s_j	$-c_{j;\uparrow} c_{j;\downarrow}$	
n^b_j	$c^\dagger_j \frac{\sigma^0}{2} c_{j+1} + \mathrm{H.c.}$	
J_j	$c^\dagger_j \frac{i\sigma^0}{2} c_{j+1} + \mathrm{H.c.}$	
$\Delta^{b,s}_j$	$c^T_j\, i\tau_y \frac{\tau^0}{2} c_{j+1}$	
Δ^b_j	$c^T_j\, i\tau_y \frac{\boldsymbol{\tau}}{2} c_{j+1}$	

opens additional channels. It is natural to study those wave vectors Q that maximize the nesting between edge states with opposite chiral eigenvalue. At half filling, this fixes $Q=\pi$. Projecting $\mathbf{S}_\pi^{(\Psi)}$ on the Majorana states generates nontrivial operators for the x and z but a vanishing y component, complementary to $Q=0$.

The MF decoupling $\mathbf{g}(S_\pi^{x,(\Psi)},S_0^{y,(\Psi)},S_\pi^{z,(\Psi)})^{\mathrm{T}}$ generates the Majorana masses

$$\frac{1}{2}\sum_{k_\parallel=0}^{\pi}\tilde{\Gamma}_{k_\parallel}^{\dagger}\left(g_{k_\parallel}^{x}\tau^{x}+\tilde{\mathbf{g}}_{k_\parallel}\boldsymbol{\tau}\right)\tilde{\Gamma}_{k_\parallel}+\cdots, \tag{4}$$

with $\tilde{\Gamma}_{k_\parallel}^{\dagger}=(\gamma_{k_\parallel}^{\dagger},-i\,s_{k_\parallel}\gamma_{k_\parallel-\pi}^{\dagger})$, $g_{k_\parallel}^{x}=\phi_{k_\parallel}^{2}(i_{\perp,0})g^{x}$, and $\tilde{\mathbf{g}}=\phi_{k_\parallel}^{2}(i_{\perp,0})\mathbf{g}\times\mathbf{e_x}$. At half filling, we make use of a sublattice symmetry $U^{\mathrm{SL}}=\sum_{k_\parallel,i_\perp}(-1)^{i_\perp}\Psi_{k_\parallel,i_\perp}^{\dagger}\frac{\tau^{x}}{2}\Psi_{k_\parallel+\pi,i_\perp}$. This symmetry generates rotations in the (y,z) plane that change the orientation of $\tilde{\mathbf{g}}$, but leave $|\tilde{\mathbf{g}}|$ and g_x invariant. Hence, there is a competition between these two channels. Interestingly, the sublattice symmetry combines a time-reversal and a translation-symmetry-breaking sector in $\tilde{\mathbf{g}}$.

As before, we rewrite Eq. (4) in terms of fermionic operators, the result of which is shown in Table I. We obtain linear superpositions of normal and SC operators. $S_\pi^{x,(\psi)}$ combines finite-momentum s-wave pairing with a bond-density-wave instability, $S_0^{y,(\psi)}$ contains complex s-wave SC and edge current operators, and $S_\pi^{z,(\psi)}$ includes a CDW instability and finite-momentum singlet SC on nearest-neighbor bonds.

Doping the system breaks the symmetry U^{SL}. As a result, the constraint on $S^{y,(\psi)}$ and $S^{z,(\psi)}$ is lifted, which allows for a competition between both channels. As the bulk nodes move away from 0 or π, the nesting wave vector Q decreases and we expect instabilities in the $S^{x,(\psi)}$ and $S^{z,(\psi)}$ channel at $Q<\pi$.

Method. We use a continuous-time QMC method in the interaction expansion [26,27]. To incorporate d-wave SC, we formulate the simulation in the Nambu basis. We perform the calculations using an effectively one-dimensional Green's function, which contains the degrees of freedom of the two-dimensional bulk states [45–47]. For more details on the QMC method, we refer the reader to Sec. III of Ref. [44]. The single particle spectra $A_{\mathrm{tot}}(\omega,k)=-(2\pi)^{-1}\sum_\sigma \mathrm{Im}\,G_\sigma(\omega,k)$ are extracted from the time-ordered Green's function $\langle c_{k,\sigma}^{\dagger}(\tau)c_{k,\sigma}(0)\rangle$ using the stochastic maximum entropy method [48,49]. To identify the mentioned Majorana masses, we determine equal-time correlation functions

$$C_{\mathcal{A},\mathcal{B}}(q)=\frac{1}{L}\sum_{n,n'}^{L}e^{iq(n-n')}(\langle\mathcal{A}_n^{\dagger}\mathcal{B}_{n'}\rangle-\langle\mathcal{A}_n^{\dagger}\rangle\langle\mathcal{B}_{n'}\rangle). \tag{5}$$

Results. The QMC simulation is sign-problem free for attractive interactions ($U=-2$) at half filling such that we can perform a scaling analysis and extrapolate to the thermodynamic limit. Doping and/or repulsive interaction introduce a sign problem. Hence, we only extract leading instabilities for $L=32$ and $U=\pm1$.

Attractive interactions. We first study the system at half filling and $\beta/t=100$. The single particle spectrum is shown in Fig. 1(a). We observe that the zero-energy flat bands develop a dispersion and gap out. Hence the interaction along the edge dynamically generates Majorana masses. The masses discussed above can generate this spectrum and lead to an unique set of coherent fermionic correlations. Figures 1(b)–1(d) suggest instabilities associated with both $|g^x|\neq0$ ($S_\pi^{x(\Psi)}$ channel) and $|\tilde{\mathbf{g}}|\neq0$ ($S_0^{y(\Psi)}$ and $S_\pi^{z(\Psi)}$ channel). Each nontrivial cross correlation confirms the expected coherent superposition of normal and SC correlations. Figure 2 visualizes the scaling behavior of the correlation function for the CDW, representing the $\tilde{\mathbf{g}}$ channel, and for s-wave singlet SC, representing the g^x channel. The data suggest long-range order at $T=0$ in the $\tilde{\mathbf{g}}$ channel, whereas g^x vanishes. Observe that we employed the enhanced symmetry of the zero-energy subspace (i.e., the chiral nature of the edge states) to derive the fermionic correlation functions associated to each Majorana mass. However, this symmetry does not manifest itself for the order parameter as it would unify the three channels by promoting the $U(1)$ sublattice symmetry to a $SU(2)$ symmetry.

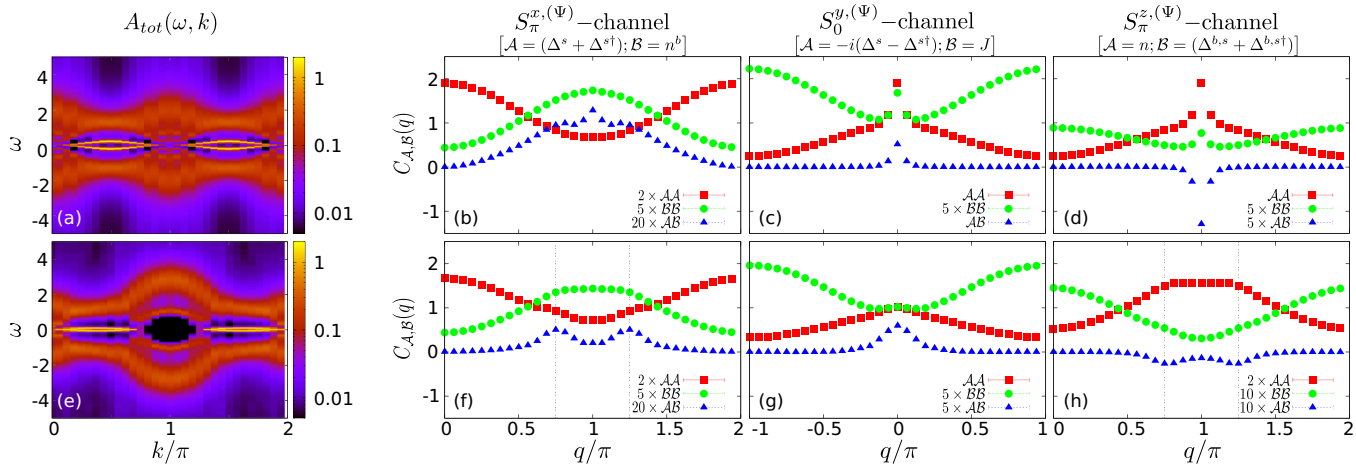

FIG. 1. We present the single particle spectrum $A_{\mathrm{tot}}(\omega,k)$ and equal-time correlation functions for attractive interactions with $L=32$ and $(U,\mu,\beta/t)=(-2,0,100)$ in the top [(a)–(d)] and $(U,\mu,\beta/t)=(-1,-0.586,50)$ in the bottom [(e)–(h)]. The edge states have been gapped out and instabilities can be identified in all three $\mathbf{S}^{(\Psi)}$ channels as defined in Table I.

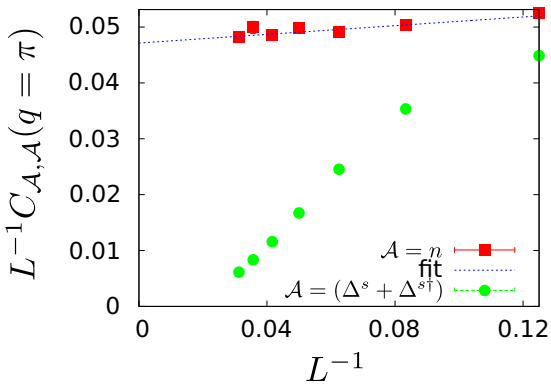

FIG. 2. Finite size scaling of $|\tilde{\mathbf{g}}|^2$ (red) and $|g^x|^2$ (green) with fixed $\beta = \frac{50}{8}L$ in red and green. The extrapolation for $\mathcal{A} = n$ suggests long-range order ($|\tilde{\mathbf{g}}| \neq 0$) at $T = 0$.

Doping the system removes the sublattice symmetry and allows a competition between the $S_0^{y(\Psi)}$ and $S_Q^{z(\Psi)}$ channels. Figure 1(e) shows the single particle spectrum and we again observe a splitting of the flat band. Once more the correlation function in Figs. 1(f)–1(h) show instabilities in all channels, which are best seen in the cross correlations between normal and SC contributions. The doping of $\mu = -0.586$ induces $Q = \pm\frac{3}{4}\pi$, which explains the instabilities in the $S^{x(\Psi)}$ and $S^{z(\Psi)}$ channels.

Repulsive interactions. The results for $L = 32$ and $\beta = 100$ are shown in Fig. 3. Again, the Majorana states are gapped out. We can confirm edge FM as the leading instability [9]. In contrast to previous studies, however, we find from the MF analysis that the FM is coherently mixed with a (anti)parallel polarized triplet SC. This is well confirmed by the correlation functions depicted in Fig. 3(b).

Discussion. Previous MF studies proposed ferromagnetism or additional is-wave pairing [4–9] along the edge as leading instabilities. Our unbiased QMC results, together with a refined MF analysis, show, however, that is-wave pairing and the FM are coherently mixed with current order and spin-triplet pairing, respectively. That is, the order parameters are linear superpositions of both normal conducting and superconducting operators, as shown by the nontrivial cross correlations (e.g., between the spin polarization and triplet pairing) in Figs. 1(b)–1(d), 1(f)–1(h), and 3(b). Indeed, the key insight from the MF analysis is that the instabilities correspond to Majorana mass terms, which in the fermionic language correspond to superpositions of particle-particle and particle-hole channels. This coherent superposition is a direct consequence of the chiral nature of the Majorana edge state. If there were both chiralities at one edge, the linear combination would be lost. Hence probing the coherence between the different fermionic order parameters provides useful information about the character of the edge states.

The agreement of the MF considerations and the QMC analysis is remarkable considering that the former completely neglected all bulk state effects. We effectively projected $\mathcal{H}_{\text{int}} \sim (e^\dagger + b^\dagger)(e + b)(e^\dagger + b^\dagger)(e + b)$ to $e^\dagger e e^\dagger e$ and ignored all bulk state contributions. Here, b and e represent bulk and edge degrees of freedom, respectively, where e has definite chirality. In principle, higher-order contributions could allow for chirality flipping pair-scattering terms which might also split the edge states [50]. The d_{xy}-wave SC is nodal and therefore hosts gapless excitations in its bulk. Accordingly, there is no separation in energy which justifies these approximations.

To detect the coherence between the FM and triplet SC in the Majorana masses, relevant for repulsive interactions (the most likely scenario for underdoped YBCO cuprate), we propose Josephson current measurements in SC-FM-SC junctions [51]. It would be useful to compare the currents in junctions where the interface is aligned along the (110) direction (with edge states) to those in junctions with an interface along the (100) direction (no edge states). The polarization direction of the FM can be controlled in this setup by applying an external magnetic field. We expect that in this junction the ferromagnetic part of the Majorana mass is aligned with the FM of the junction. This also fixes the polarization of the triplet component to be either parallel or antiparallel to the FM, depending on the orientation (see Table I). This polarization direction is expected to strongly influence the tunneling probability and therefore the Josephson current. By varying the polarization of the FM, one can manipulate the relative phase in the superposition between the FM and the triplet pairing, such that we would not only detect the presence of additional triplet pairing along the edge but also infer information about the coherence between the different components.

In the presence of attractive interactions, the CDW order will be pinned by impurities or by the underlying lattice [52]. Thereby, charge modulations in STM should be observable.

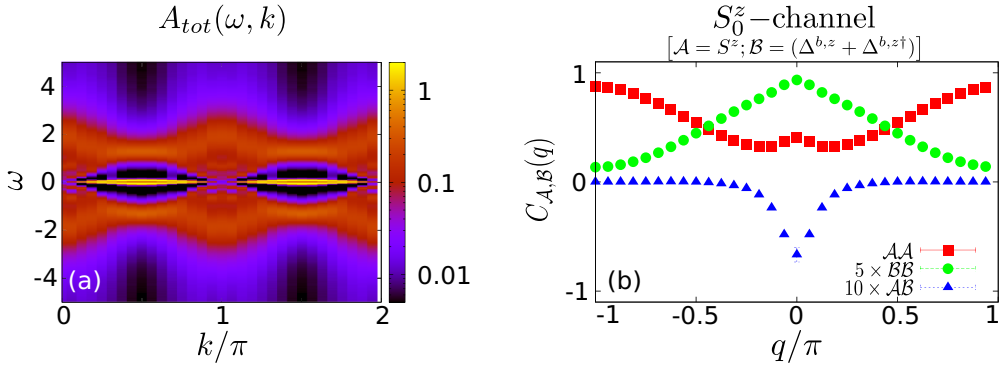

FIG. 3. We present the single particle spectrum $A_{\text{tot}}(\omega,k)$ (a) and the correlation functions (b) for $L = 32$ and $\beta/t = 100$. The edge states have been gapped out and the FM is coherently mixed with triplet SC.

Summary. In this Rapid Communication, we have studied instabilities of chiral flat-band Majorana fermions in topological SCs using QMC. We have confirmed the FM instability for repulsive interactions beyond the mean-field level. Our analysis points out that any normal conducting order is coherently mixed with a SC counterpart due to the Majorana nature of the edge states, for example, FM and triplet SC. This mixing should open up possibilities to detect the instabilities experimentally. In the case of attractive interactions, the system exhibits long-range order at half filling and $T = 0$, namely, CDW combined with finite-momentum extended s-wave pairing and complex s-wave SC in superposition with current order. In a doped system, these two orders compete with each other and the numerical data suggest an instability towards SC mixed with spontaneous edge currents.

Acknowledgments. The authors thank P. Brouwer, P. Brydon, F. Goth, M. Hohenadler, E. Khalaf, R. Queiroz, C. Timm, and M. Weber for useful discussions. J.H. and F.A. are supported by the German Research Foundation (DFG), under DFG-SFB 1170 "ToCoTronics" (Project C01) and DFG-FOR 1162 (AS120/6-2). We thank the Jülich Supercomputing Centre for generous allocation of CPU time.

[1] M. Z. Hasan and C. L. Kane, Rev. Mod. Phys. **82**, 3045 (2010).
[2] X.-L. Qi and S.-C. Zhang, Rev. Mod. Phys. **83**, 1057 (2011).
[3] C.-K. Chiu, J. C. Y. Teo, A. P. Schnyder, and S. Ryu, Rev. Mod. Phys. (to be published), arXiv:1505.03535.
[4] M. Matsumoto and H. Shiba, J. Phys. Soc. Jpn. **64**, 3384 (1995).
[5] M. Matsumoto and H. Shiba, J. Phys. Soc. Jpn. **64**, 4867 (1995).
[6] M. Fogelström, D. Rainer, and J. A. Sauls, Phys. Rev. Lett. **79**, 281 (1997).
[7] C. Timm, S. Rex, and P. M. R. Brydon, Phys. Rev. B **91**, 180503(R) (2015).
[8] C. Honerkamp, K. Wakabayashi, and M. Sigrist, Europhys. Lett. **50**, 368 (2000).
[9] A. C. Potter and P. A. Lee, Phys. Rev. Lett. **112**, 117002 (2014).
[10] N. B. Kopnin, T. T. Heikkilä, and G. E. Volovik, Phys. Rev. B **83**, 220503(R) (2011).
[11] G. Z. Magda, X. Jin, I. Hagymási, P. Vancsó, Z. Osváth, P. Nemes-Incze, C. Hwang, L. P. Biró, and L. Tapasztó, Nature (London) **514**, 608 (2014).
[12] H. Feldner, Z. Y. Meng, A. Honecker, D. Cabra, S. Wessel, and F. F. Assaad, Phys. Rev. B **81**, 115416 (2010).
[13] H. Feldner, Z. Y. Meng, T. C. Lang, F. F. Assaad, S. Wessel, and A. Honecker, Phys. Rev. Lett. **106**, 226401 (2011).
[14] B. Roy, F. F. Assaad, and I. F. Herbut, Phys. Rev. X **4**, 021042 (2014).
[15] E. Tang and L. Fu, Nat. Phys. **10**, 964 (2014).
[16] A. H. Castro Neto, F. Guinea, N. M. R. Peres, K. S. Novoselov, and A. K. Geim, Rev. Mod. Phys. **81**, 109 (2009).
[17] C.-K. Chiu and A. P. Schnyder, Phys. Rev. B **90**, 205136 (2014).
[18] Y. Tanaka, M. Sato, and N. Nagaosa, J. Phys. Soc. Jpn. **81**, 011013 (2012).
[19] S. Matsuura, P.-Y. Chang, A. P. Schnyder, and S. Ryu, New J. Phys. **15**, 065001 (2013).
[20] A. P. Schnyder and P. M. R. Brydon, J. Phys.: Condens. Matter **27**, 243201 (2015).
[21] A. P. Schnyder and S. Ryu, Phys. Rev. B **84**, 060504(R) (2011).
[22] S. Ryu and Y. Hatsugai, Phys. Rev. Lett. **89**, 077002 (2002).
[23] Y. Tanaka, T. Yokoyama, A. V. Balatsky, and N. Nagaosa, Phys. Rev. B **79**, 060505(R) (2009).
[24] Y. Li, D. Wang, and C. Wu, New J. Phys. **15**, 085002 (2013).
[25] V. J. Kauppila, T. Hyart, and T. T. Heikkilä, Phys. Rev. B **93**, 024505 (2016).
[26] A. N. Rubtsov, V. V. Savkin, and A. I. Lichtenstein, Phys. Rev. B **72**, 035122 (2005).
[27] E. Gull, A. J. Millis, A. I. Lichtenstein, A. N. Rubtsov, M. Troyer, and P. Werner, Rev. Mod. Phys. **83**, 349 (2011).
[28] E. Pavarini, E. Koch, D. Vollhardt, and A. Lichtenstein, *DMFT at 25: Infinite Dimensions—Lecture Notes of the Autumn School on Correlated Electrons 2014* (Verlag Forschungszentrum Jülich, Jülich, 2014).
[29] P. A. Lee, N. Nagaosa, and X.-G. Wen, Rev. Mod. Phys. **78**, 17 (2006).
[30] D. J. Scalapino, Phys. Rep. **250**, 329 (1995).
[31] J. Geerk, X. X. Xi, and G. Linker, Z. Phys. B **73**, 329 (1988).
[32] J. Lesueur, L. H. Greene, W. L. Feldmann, and A. Inam, Physica C: Superconductivity **191**, 325 (1992).
[33] M. Covington, R. Scheuerer, K. Bloom, and L. H. Greene, Appl. Phys. Lett. **68**, 1717 (1996).
[34] S. Kashiwaya, Y. Tanaka, M. Koyanagi, H. Takashima, and K. Kajimura, Phys. Rev. B **51**, 1350 (1995).
[35] L. Alff, H. Takashima, S. Kashiwaya, N. Terada, H. Ihara, Y. Tanaka, M. Koyanagi, and K. Kajimura, Phys. Rev. B **55**, R14757(R) (1997).
[36] J. Y. T. Wei, N.-C. Yeh, D. F. Garrigus, and M. Strasik, Phys. Rev. Lett. **81**, 2542 (1998).
[37] S. Kashiwaya and Y. Tanaka, Rep. Prog. Phys. **63**, 1641 (2000).
[38] M. Covington, M. Aprili, E. Paraoanu, L. H. Greene, F. Xu, J. Zhu, and C. A. Mirkin, Phys. Rev. Lett. **79**, 277 (1997).
[39] R. Krupke and G. Deutscher, Phys. Rev. Lett. **83**, 4634 (1999).
[40] Note that splitting of the zero-bias peak at low temperatures was not confirmed in all experiments (see, e.g., Ref. [53]).
[41] A. P. Schnyder, S. Ryu, A. Furusaki, and A. W. W. Ludwig, Phys. Rev. B **78**, 195125 (2008).
[42] A. Y. Kitaev, Phys. Usp. **44**, 131 (2001).
[43] A. P. Schnyder, P. M. R. Brydon, and C. Timm, Phys. Rev. B **85**, 024522 (2012).
[44] See Supplemental Material at http://link.aps.org/supplemental/10.1103/PhysRevB.93.201116 for a derivation of the edge-state wave function, the details of the mean field calculation, and a description of the Quantum Monte Carlo Method.
[45] M. Hohenadler, T. C. Lang, and F. F. Assaad, Phys. Rev. Lett. **106**, 100403 (2011).
[46] M. Hohenadler and F. F. Assaad, Phys. Rev. B **85**, 081106(R) (2012).
[47] M. Hohenadler and F. F. Assaad, Phys. Rev. B **90**, 245148 (2014).
[48] A. W. Sandvik, Phys. Rev. B **57**, 10287 (1998).
[49] K. S. D. Beach, arXiv:cond-mat/0403055.

[50] R. Queiroz and A. P. Schnyder, Phys. Rev. B **89**, 054501 (2014).

[51] A. E. Sheyerman, K. Y. Constantinian, G. A. Ovsyannikov, Y. V. Kislinskii, A. V. Shadrin, A. V. Kalabukhov, and Y. N. Khaydukov, J. Exp. Theor. Phys. **120**, 1024 (2015).

[52] P. Lee, T. Rice, and P. Anderson, Solid State Commun. **14**, 703 (1974).

[53] H. Kashiwaya, S. Kashiwaya, B. Prijamboedi, A. Sawa, I. Kurosawa, Y. Tanaka, and I. Iguchi, Phys. Rev. B **70**, 094501 (2004).